Journal of Saudi Chemical Society (2015) 19, 511–520

King Saud University

Journal of Saudi Chemical Society

www.ksu.edu.sa
www.sciencedirect.com

ORIGINAL ARTICLE

Ferric oxide nanoparticles decorated carbon nanotubes and carbon nanofibers: From synthesis to enhanced removal of phenol

Hamza A. Asmaly [a], Basim Abussaud [b,*], Ihsanullah [b], Tawfik A. Saleh [c], Vinod Kumar Gupta [d,e,f], Muataz Ali Atieh [g,*]

[a] *King Abdulaziz City for Science and Technology – Technical Innovation Center on Carbon Capture and Sequestration, King Fahd University of Petroleum and Minerals, Saudi Arabia*
[b] *Department of Chemical Engineering, King Fahd University of Petroleum & Minerals, Dhahran 31261, Saudi Arabia*
[c] *Chemistry Department, King Fahd University of Petroleum & Minerals, Dhahran 31261, Saudi Arabia*
[d] *Department of Chemistry, Indian Institute of Technology Roorkee, Roorkee 247667, India*
[e] *Centre for Environment and Water, The Research Institute, King Fahd University of Petroleum and Minerals, Dhahran, Saudi Arabia*
[f] *Department of Applied Chemistry, University of Johannesburg, Johannesburg, South Africa*
[g] *Qatar Environment and Energy Research Institute, Qatar Foundation, PO Box 5825, Doha, Qatar*

Received 17 February 2015; revised 4 June 2015; accepted 8 June 2015
Available online 16 June 2015

KEYWORDS

Carbon fibers;
Carbon nanotubes;
Ferric oxide impregnation;
Phenol;
Removal

Abstract In this work, ferric oxide nanoparticle decorated carbon fibers and carbon nanotubes (CNF/Fe_2O_3 and CNT/Fe_2O_3) were synthesized and characterized by scanning electron microscopy (SEM), thermogravimetric analysis (TGA), energy dispersive X-ray spectroscopy (EDS), transmission electron microscopy (TEM), X-ray diffraction (XRD), zeta potential and BET surface area analyzer. The prepared nanocomposites were evaluated or the removal of phenol ions from aqueous solution. The effects of experimental parameters, such as shaking speed, pH, contact time, adsorbent dosage and initial concentration, were evaluated for the phenol removal efficiency. The adsorption experimental data were represented by both the Langmuir and Freundlich isotherm models. The Langmuir isotherm model best fitted the data on the adsorption of phenol, with a high correlation coefficient. The adsorption capacities, as determined by the Langmuir isotherm model were

* Corresponding authors. Tel.: +966 1 38602205; fax: +966 1 38604234.
E-mail address: motazali@kfupm.edu.sa (M.A. Atieh).
Peer review under responsibility of King Saud University.

Production and hosting by Elsevier

http://dx.doi.org/10.1016/j.jscs.2015.06.002

0.842, 1.098, 1.684 and 2.778 mg/g for raw CNFs, raw CNTs, CNF–Fe_2O_3 and CNT–Fe_2O_3, respectively.

1. Introduction

Phenolic compounds are generated in pulp and paper, petroleum refinery, dye synthesis, coal gasification and pharmaceutical industries and have been identified as common contaminants in wastewaters. Phenols have found application in the production of wide varieties of phenolic resins, used in construction of automobiles and appliances, adhesives and epoxy resins, as well other various applications [1]. Due to the harmful nature of phenols and their potential hazardous effects on human health, they have been classified as toxic pollutants. Hence, it is required by the US Environmental Protection Agency (EPA) regulations to lower phenol content of wastewater below 1 ppm [2].

Various techniques have been developed for the phenol removal from wastewater, such as electrochemical oxidation [5], adsorption [3–6], wet air oxidation [7,8], chemical coagulation [9], solvent extraction [10], membrane separation [11,12], bioremediation [13,14] and photo catalytic degradation [15,16]. Traditionally, activated sludge has been widely employed for the removal of phenol from wastewater because of its relatively low cost and straightforward process [17]. However, this method is not efficient for the treatment of wastewater with high concentration of phenol due to low biodegradability. In addition, the regeneration process of the adsorbent is not only expensive, but also very complex [3,18].

The application of adsorption for phenol treatment in wastewater is favored by its potential to remove both organic and inorganic constituents, even at low concentrations. Adsorption has the advantage of its relative ease of operation both in batch and continuous operation, the absence of sludge formation, potential of regenerative reuse of adsorbent and availability of low cost adsorbent materials [12]. Carbon-based adsorbent materials, which are hydrophobic and non-polar, have good potential for phenol removal in wastewater. Their large surface area, well developed porosity and tunable surface-containing functional groups are features that enhanced their adsorption efficiency [12,13].

Various nanomaterials have been investigated recently for prudential applications in various fields. Carbon nanotubes have been employed for the removal of heavy metals [18] and organic compounds [19] from water. Metal oxides decorated with metal particles have shown photocatalytic, optical and visible light photoelectrochemical performance [20–23].

In this work, ferric oxide impregnated carbon fibers and carbon nanotubes were employed for the removal of phenol from water. Surface of the CNFs and CNTs were modified with ferric oxide, to study its effect on phenol adsorption. The physicochemical properties of the modified and unmodified CNFs and CNTs were determined using SEM, EDS, TEM, XRD, zeta potential, BET surface area analysis and TGA. The effects of experimental parameters, such as adsorbent dosage, contact time, pH, initial phenol concentration and shaking speed on the removal of phenol, were investigated.

2. Experimental

2.1. Adsorbent impregnation

Carbon fibers (CNFs) and carbon nanotubes (CNTs) used in this study were purchased from Nanostructured and Amorphous Materials, Inc. USA. The CNFs had 95% purity, outside diameter of 200–500 nm and length ranging from 10 to 40 μm, while the CNTs had 95% purity, outside diameter of 10–20 nm and length ranging from 1 to 10 μm.

Ferric oxide (Fe_2O_3) from ferric nitrate Fe $(NO_3)_2{\cdot}6H_2O$ was impregnated onto 5 g of the CNFs and CNTs in ethanol (98% purity), followed by sonication (110 V at 40% amplitude) and calcination at 350 °C for 3 h. For 10% iron oxide 1.443 g of pure ferric nitrate [Fe $(NO_3)_3{\cdot}9H_2O$] was dissolved in 300 mL ethanol. An amount of 1.8 of CNTs/CNFs was also dissolved in 400 mL of absolute ethanol. Both solutions were sonicated for 45 min separately and then mixed together. The resultant mixture was again sonicated for 1 h at room temperature. The mixture was then kept in an oven to evaporate the ethanol. The aim of ultrasonication is to have a complete and homogeneous wetting of the particles during impregnation and hence decreasing the possibility of agglomeration due to the formation of clumps of liquid [9]. The residue was then calcinated for 3.5 h at 350 °C in furnace to get CNTs/CNFs impregnated with 1% iron oxide.

2.2. Characterization

The prepared materials have been characterized using scanning electron microscopy–energy dispersive X-ray spectroscopy (SEM–EDS), Back scattering FE-SEM, TEM, thermogravimetric analysis (TGA), BET surface area analyzer Micrometrics ASAP 2020, zeta potential, and X-ray diffraction (XRD).

2.3. Preparation of stock solution

Stock solution of phenol with initial concentration of 2 ppm was prepared by serial dilution of 1000 ppm solution. First 1000 mg of phenol was dissolved in 1 L deionized water. Solvents (1.0 M nitric acid and 1.0 M sodium) were used to adjust pH of the stock solution. Solution pH was maintained during the experiments by the addition of buffer solutions.

2.4. Batch adsorption studies

Batch adsorption experiments were performed at room temperature to study the effects of pH, contact time, adsorbent dosage and shaking speed on the phenol adsorption efficiency by the raw and decorated ones with ferric oxide (CNF–Fe_2O_3). The concentrations of phenol were analyzed using UV–VIS and the percentage removal was calculated as:

$$\text{Percentage Removal} = \frac{C_i - C_e}{C_i} \times 100 \quad (1)$$

$$\text{Adsorption Capacity, } q_e\,(\text{mg/g}) = \frac{C_i - C_e}{M_s} \times V \quad (2)$$

where C_i is the initial concentration of phenol ions in the solution (mg/L), C_e is the concentration of phenol ions in solution (mg/L), V is the total volume of solution (L) and M_S is the carbon dosage (g).

2.5. Adsorption isotherm models

The Langmuir isotherm model is based on the assumption of monolayer adsorption from the homogenous surface. While Freundlich isotherm model assumes adsorption from heterogeneous surface, with non uniform heat distribution on the surface.

The Langmuir and Freundlich models can be expressed mathematically by Eqs. (3) and (4), respectively:

$$\frac{C_e}{Q_e} = \frac{1}{Q_{\max} K_L} + \frac{C_e}{Q_{\max}} \quad (3)$$

$$\text{Log}\, Q_e = \text{Log}\, K_f + \left(\frac{1}{n}\right) \text{Log}\,(C_e) \quad (4)$$

where Q_e (mg/g) = amount adsorbed (mg/g). C_e (mg/L) = equilibrium concentration of phenol in the liquid phase. Q_m (mg/g) = maximum adsorption capacity. K_L = Langmuir constant. K_f and n are the Freundlich constants.

3. Results and discussions

3.1. Characterization

3.1.1. Scanning electron microscopy–energy dispersive X-ray spectroscopy (SEM–EDS)

The raw and ferric oxide decorated carbon fibers (CNF–Fe_2O_3) and carbon nanotubes (CNT–Fe_2O_3) were characterized using scanning electron microscopy (SEM).

Fig. 1 shows the SEM images of raw and doped CNFs. The elemental composition of the CNF–Fe_2O_3 was obtained using the EDS, and showed the presence of metal oxide nanoparticles on CNFs. Table 1 shows a summary of the results of EDS analysis, while Fig. 2 shows EDS spectrum of CNF–Fe_2O_3. It was observed that the oxygen content of the CNF–Fe_2O_3 is higher than that of the raw CNFs, which is attributed to the presence of oxygen containing metal oxide to CNF surface.

Fig. 1(c and d) displays the SEM images of CNTs and CNT–Fe_2O_3. The white spots in the SEM image of CNT–Fe_2O_3 show the iron oxide particles, as confirmed by EDS analysis. The outcome of the analysis is shown as EDS spectrum in Fig. 2b. Table 1 indicates the weight percentages of the elements.

Back scattering FE-SEM image of CNT–Fe_2O_3 was taken in order to verify the presence of nanoparticles ions on the surfaces of the CNTs as shown in Fig. 3a. The distribution of Fe_2O_3 nanoparticles on the nanotube surface was observed as white crystal structures of Fe_2O_3 nanoparticles with a small average size. It can be seen that Fe_2O_3 nanoparticles spread widely on the surfaces of carbon nanotubes forming small crystal particles with diameters varying from 1 to 5 nm. TEM was used to characterize the structure and size of nanotubes and iron nanoparticles on the surfaces. Fig. 3b and c shows TEM images of raw and doped CNTs. It was found that the iron nanoparticles cover the surfaces the CNTs with an average particle size ~6 nm. TEM image of raw CNTs (Fig. 3b) shows that it is a highly ordered structure with a diameter range of 10–30 nm. Fig. 3c shows the TEM image of CNTs impregnated with iron nanoparticles. The diameter of the Fe_2O_3 nanoparticles ranges from 1 to 2 nm with spherical shape and homogeneous distribution.

3.1.2. Thermogravimetric analysis (TGA)

The raw and ferric oxide decorated carbon fibers (CNF–Fe_2O_3) and carbon nanotubes (CNT–Fe_2O_3) were characterized using thermogravimetric analysis (TGA). The analysis was performed under air with a heating rate of 10 °C/min.

As shown in Fig. 4a, the initial degradation of CNF–Fe_2O_3 is lower than raw CNFs. The sample weight is reduced to almost 0.32% and 3% for CNFs and CNF–Fe_2O_3, respectively at 900 °C. This is due to the fact that all carbonaceous materials have been removed and a small amount of metal is left behind. Thermal degradation of the raw and impregnated CNTs was studied using thermogravimetric analysis (TGA). Fig. 4 shows the TGA curves for the CNTs and CNT–Fe_2O_3 under air with a heating rate of 10 °C/min. The initial degradation temperature of CNTs was found to be 550 °C, while the maximum weight loss occurred at about 600 °C and degradation completes at about 670 °C. While for CNT–Fe_2O_3, the initial oxidation temperatures start at 500 °C, reaching a maximum weight loss of at about 550 °C. It can also be observed that the amount reaming after heating the CNTs and CNFs up to 900 °C is higher than the raw forms of CNTs and CNFs. This may be attributed to the iron oxide content that is left behind after evaporation of carbon material.

3.1.3. Brunauer Emmett Teller (BET) surface area analysis

Surface area of the CNFs, CNT–Fe_2O_3 and CNF–Fe_2O_3 was measured using BET surface area analyzer Micrometrics ASAP 2020. The results are interpreted based on the adsorption–desorption of N_2 at 77 K. The BET surface area values obtained for the CNTs and CNT–Fe_2O_3 were 155.5 and 227.5 m^2/g, respectively, as shown in Fig. 4c–d. The BET surface area of the CNFs and CNF–Fe_2O_3 was found to be 40.7 and 72.4 m^2/g, respectively. The high surface area of CNF–Fe_2O_3 suggests that additional adsorption sites are available due to attachment of Fe_2O_3 nanoparticles to CNFs surface. The BET surface area values obtained for the CNTs and CNT–Fe_2O_3 were 155.5 and 227.5 m^2/g, respectively. This indicated that the iron oxide nanoparticles doped on the surface of CNTs, as shown by SEM and TEM images, enhanced their surface area and hence increased the number of sites for adsorption.

3.1.4. Zeta potential

Zeta potential can be used to measure the electrical potential on the adsorbent surface. From the values of zeta potential at different pH, surface acidity or basicity and isoelectric point can be determined. The values of the zeta potential can also be used to predict the stability of colloidal dispersions. It is a

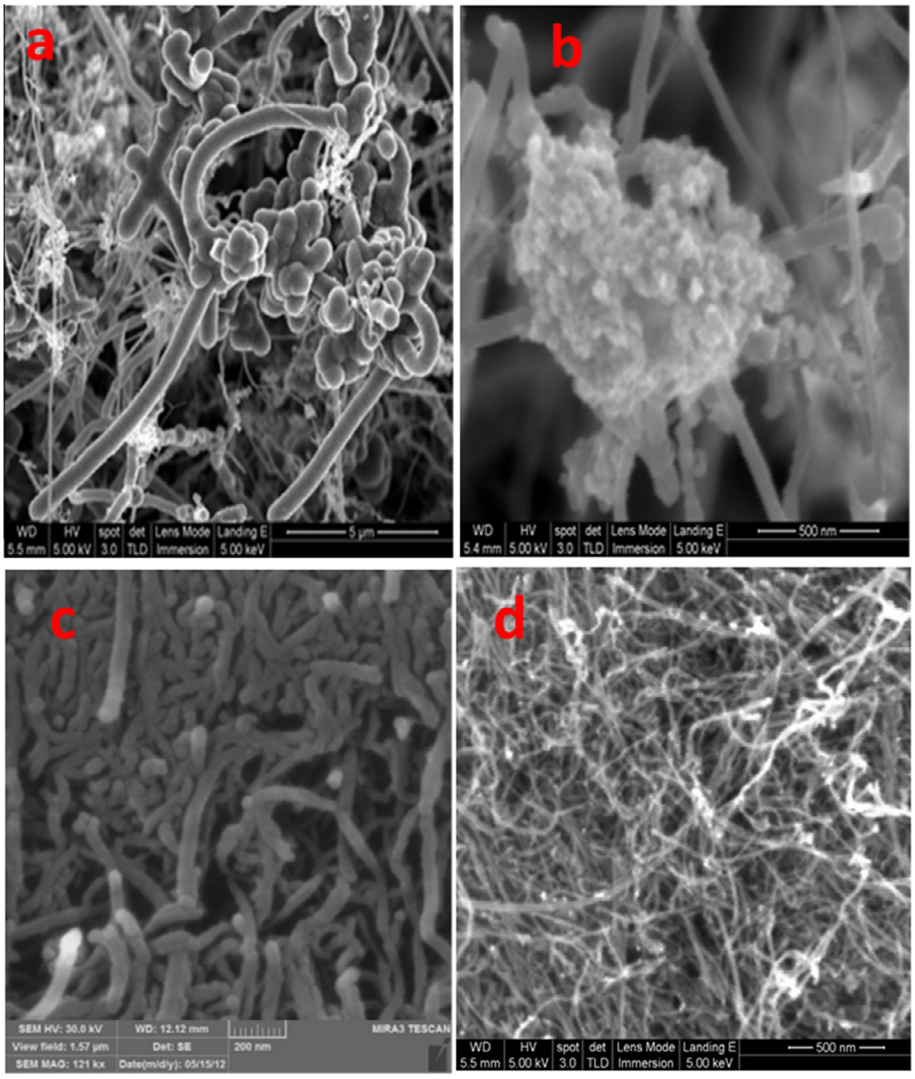

Figure 1 SEM micrographs of (a) raw CNFs (b) CNF–Fe_2O_3(c) pure CNTs (d) CNT–Fe_2O_3.

Table 1 EDS analysis of CNFs, CNF–Fe_2O_3, CNTs and CNT–Fe_2O_3.

Element	Raw CNFs	CNF–Fe_2O_3	Raw CNT	CNT–Fe_2O_3
C	97.86	91.41	98.50	83.65
O	1.82	6.13	3.50	14.01
Fe	–	2.14	–	2.34
Total%	100	100	100	100

measure of the degree of repulsion between similarly charged particles. Zeta potential of the regular and impregnated CNTs has been measured using Zeta Sizer Nano Z from Malvern. Particles with low values of zeta potential will agglomerate, while high zeta potential particles are electrically stable.

The value of zeta potential for pure CNTs was higher than CNT–Fe_2O_3, so it will tend to aggregate in solution forming big particles due to strong van der Waals interaction between the particles. It can also be observed that the pH of the solution also affects the zeta potential values by changing the nature of particles in the solution. Impregnation of CNTs has reduced the zeta potential values and phenol ions' adsorption efficiency, increased due to electrostatic interaction of phenol ions and CNT surface.

3.1.5. X-ray diffraction (XRD)

The XRD patterns were recorded using X-ray diffractometer, equipped with Cu KR radiation (40 kV, 20 mA) at a rate of 1.0°/min over the range of 10–80° (2α). The XRD pattern for the doped CNTs indicated that there is one characteristic peak of CNTs that was observed at 2θ of 27, while other characteristic peaks were found at 2θ, 34.36, 42, 50, 54, 63, 65, 72 and 75 which correspond to Fe_2O_3. These results revealed that the Fe_2O_3 particles were successfully attached to the CNTs.

3.2. Effect of operating variables

3.2.1. Effect of pH

The solution pH is a critical variable in the adsorption of ions from aqueous solution. It influences not only the surface

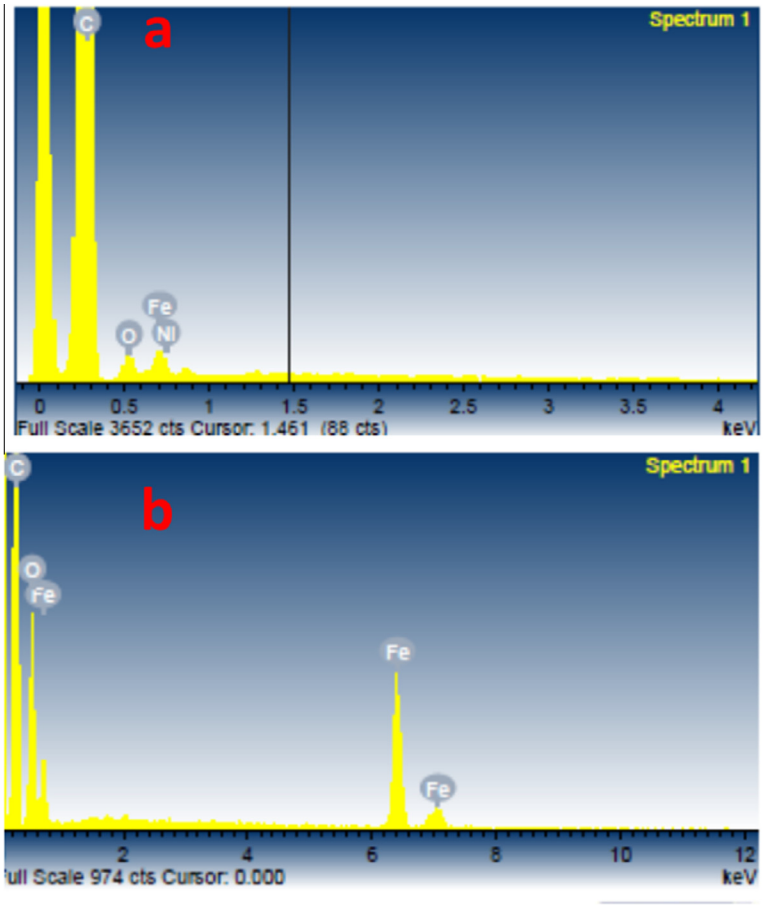

Figure 2 EDS spectrum of CNF–Fe_2O_3 and CNT–Fe_2O_3.

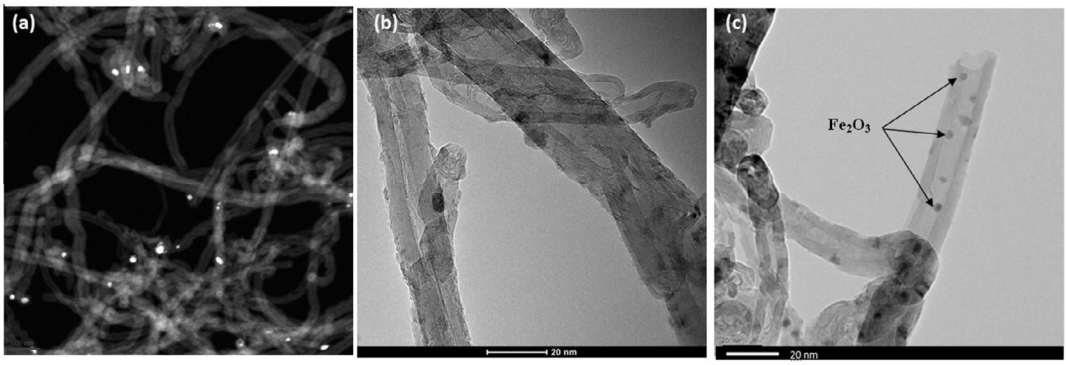

Figure 3 (a) Back scattering FE-SEM images for CNT–Fe_2O_3 (b) TEM image of CNTs (c) TEM image of CNT–Fe_2O_3.

binding sites of the adsorbent but also the adsorbate chemistry in water. The extent of phenol removal was evaluated at a pH from 2 to 9, while all the other parameters including contact time, adsorbent dosage, and initial concentration and shacking speed were kept constant at 2 h, 50 mg, 2 ppm and 100 rpm, respectively.

The highest removal efficiency of phenol was observed at pH 7, with the percentage removal of 30.8% and 72.2% by CNFs and CNF–Fe_2O_3, respectively. However, at pH above 7, a decrease in the percentage removal was observed for both raw CNFs and CNF–Fe_2O_3.

Similarly, the extent of dephenolation by CNTs and CNT–Fe_2O_3 was also evaluated in the pH range from 2 to 9. It can be seen that the highest removal efficiency of phenol was observed at pH 7, with the percentage removal of 46% and 74.8% by CNTs and CNT–Fe_2O_3, respectively. The percentage removal of phenol remains almost constant for CNT–Fe_2O_3 at pH above 7, however, a decrease in the percentage removal was observed for raw CNTs at higher pH.

This decrease in the percentage removal of phenol at higher pH by raw CNFs can be explained on the basis of ionic chemistry of the solution and surface charge of the CNFs. Phenol is

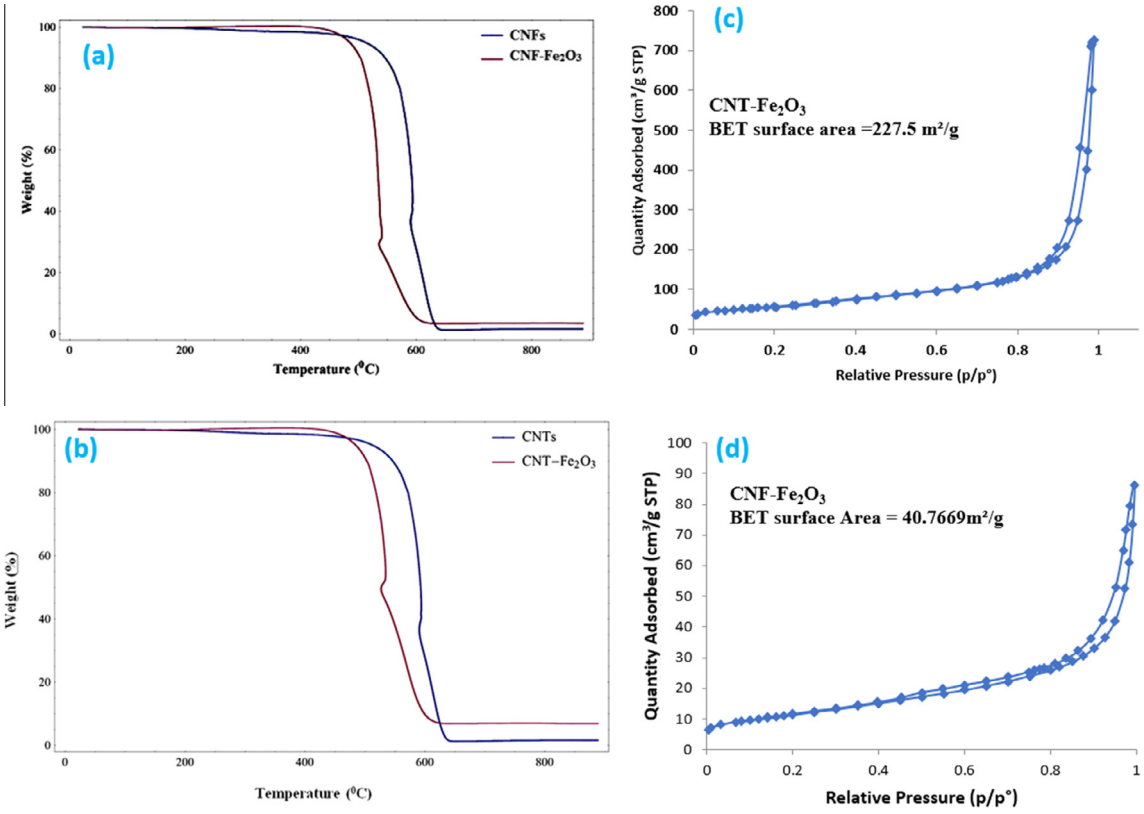

Figure 4 Thermogravimetric analysis (TGA) for (a) pure CNF, CNF–Fe_2O_3 and (b) CNT, CNT–Fe_2O_3; and adsorption–desorption curves of N_2 at 77 K for (c) CNT–Fe_2O_3 (d) CNF–Fe_2O_3.

a weak acid (p*K*a = 10) and will be adsorbed to a less extent at higher pH. Therefore, at higher pH, the repulsive forces between the negatively charged surface of CNFs and phenol are responsible for low adsorption. While at lower pH (below 7), the presence of more positive ions on the surface of CNFs, leads to electrostatic interaction with the phenolate ions and enhanced the adsorption. It is also important to note that at higher pH, some other mechanisms like physical adsorption might occur, which can also affect the ion exchange process. The removal efficiency of phenol by CNF–Fe_2O_3 is higher than CNFs for the same pH values [9,13].

The higher removal of CNT–Fe_2O_3 can be explained by its higher surface area which provides more adsorption sites for phenol ions in addition to the pi–pi electron-donor–acceptor (EDA) interaction and/or hydrophobic effect can be considered to interpret the sorption mechanisms of phenol on carbon-based materials. Banat et al., [13] and Halouli et al., [9] reported similar pH behaviors in phenol adsorption onto activated charcoal and bentonite clay, respectively.

3.2.2. Effect of shaking speed

The shaking speed is considered an important factor in the adsorption process. Agitation facilitates a proper contact between ions in the solution and adsorbent binding sites and thereby promotes effective diffusion of ions toward the adsorbent surface. The shaking speed was varied between 50 and 250 rpm. The removal efficiency of phenol increases with increase in shaking speed and maximum removal was achieved at 150 rpm for both CNFs and CNF–Fe_2O_3. This can be attributed to the effective transport of phenol ions toward the CNFs and CNF–Fe_2O_3 occurred, due to less resistance to diffusion at higher shaking speed.

However, no significant change in removal efficiency was achieved beyond 200 rpm, which might be due to the saturation of adsorption sites. It is worth mentioning that the removal by CNF–Fe_2O_3 was higher (79%) than the raw CNFs (64.6%) at the same value of shaking speed. This observation was attributed to the improved contact between the phenol ions in the solution and the presence of more active adsorption sites on the CNF–Fe_2O_3 surface [14–15]. Shaking facilitates a proper contact between ions in the solution and adsorbent binding sites and thereby promotes effective diffusion of ions toward the adsorbent surface. The range of shaking speed used in this study was from 50 to 250 rpm, while all the other parameters including contact time, adsorbent dosage, initial concentration and pH were kept constant at 150 min, 50 mg, 2 ppm and 7, respectively.

The effect of shaking speed on the removal efficiency of CNTs and CNT–Fe_2O_3 was studied. The results showed that the removal efficiency of phenol increases with increase in shaking speed and maximum removal by both CNTs and CNT–Fe_2O_3 was achieved at 150 rpm. This can be justified by the fact that an effective transport of phenol ions toward the CNTs and CNT–Fe_2O_3 occurred, due to less resistance to diffusion at higher shaking speed [14–16].

3.2.3. Effect of contact time

In order to study the effect of contact time on the removal efficiency of phenol and to determine the equilibrium time for maximum uptake of phenol ions by CNFs and CNF–Fe_2O_3, experiments were performed under contact times from 0 to 710 min. All the other parameters including shaking speed, adsorbent dosage, initial concentration and pH were kept constant at 100 rpm, 50 mg, 2 ppm and 7, respectively.

A gradual increase in phenol removal efficiency was observed to increase in time for all the adsorbents still 2 h, at which the optimum adsorption was attained. This observation was attributed to the adsorption equilibrium phenomenon, whereby the rate of adsorption was higher than the rate of desorption up to 2 h of contact time, which is the equilibrium adsorption point. At this time, the rate of adsorption and desorption were same and no further removal of phenol from the solution was achieved. Also, a clear desorption of phenol from both the adsorbents was observed after 2 h due to the saturation of the active sites on the surfaces of adsorbents. An increase in adsorption of phenol ions to increase in contact time may also be due to the decrease in boundary layer resistance of the hydrate layer [16].

Furthermore, the phenol removal efficiency of CNF–Fe_2O_3 was higher than CNFs at same contact time. The maximum phenol removal efficiency by CNF–Fe_2O_3 and CNFs was 79% and 43.6%, respectively. The phenol removal efficiency of CNT–Fe_2O_3 was higher than CNTs at same contact time. The maximum phenol removal efficiency by CNT–Fe_2O_3 and CNTs was 86.3% and 62.7%, respectively.

3.2.4. Effect of dosage

The dosages of adsorbents were varied from 10 to 500 mg, keeping all other experimental parameters constant. The percentage removal of phenol was observed to increase with an increase in the adsorbent dosages, with maximum removal at 400 and 200 mg for CNFs and CNF–Fe_2O_3, respectively. Doped CNFs removed almost 100% of phenol ions at a dosage of 200 mg, while pure CNFs were able to remove 89.3% of phenol ions at 400 mg. This showed the excellent removal efficiency of phenol by CNF–Fe_2O_3 even at lower adsorbent dosage.

There was an increase in the phenol removal efficiency with the increase in dosage to 200 and 400 mg for CNFs and CNF–Fe_2O_3, respectively. Beyond this dosage, no notable increase in removal was observed with further increase in dosage. This observation was attributed to increase in the number of active adsorption sites until the optimum dosage was attained. Removal efficiency remained constant beyond the optimum dosage of 200 and 400 mg for CNFs and CNF–Fe_2O_3, respectively. This might be due to conglomeration or overlapping of the active adsorption sites at dosages beyond the optimum [17].

The doses of the CNTs were varied from 10 to 400 mg, while all the other parameters including shaking speed, contact time, initial concentration and pH were kept constant at 150 rpm, 150 min, 2 ppm and 7, respectively. The percentage removal of phenol was observed to increase with an increase in the adsorbent dosages, with maximum removal at 350 and 200 mg for CNTs and CNT–Fe_2O_3, respectively. Doped CNTs removed almost 100% of phenol ions at a dosage of 200 mg, while the amount of pure CNTs required for complete removal of phenol ions was 350 mg. This showed almost 75% enhancements in the removal efficiency of phenol by CNT–Fe_2O_3.

3.2.5. Effect of initial concentration

The effect of the initial concentration of phenol ions on the removal extent of phenol was also studied. The initial concentration of phenol in the solution was varied between 2 and 10 ppm, while all the other parameters were kept constant during the experiment, Fig. 5. Almost 100% phenol removal was obtained using an initial concentration of 2 ppm for both CNFs and CNF–Fe_2O_3. However, increasing the initial phenol concentration in the solution resulted in a decrease in the removal efficiency of the phenol by both CNFs and CNF–Fe_2O_3.

This observation is reasonable due to the high amount of phenol ions with limited active adsorption sites on the adsorbent surfaces, which leads to increase in the concentration of phenol ions in the bulk solution and thus decreased the removal of phenol. This decrease in phenol uptake with an increase in phenol concentration is logical, because the time required to attain equilibrium was expected to be longer at higher concentrations than at lower concentration. It is interesting to note that the doped CNFs still have higher removal efficiency than the raw CNFs for the same value of initial phenol concentration. This can be justified on the basis of availability of more adsorption sites and higher surface area of CNF–Fe_2O_3. Therefore, more ions can be adsorbed on the surface compared to raw CNFs at higher phenol concentration and hence higher removal efficiency was observed. It was observed that almost 100% phenol removal was obtained using an initial concentration of 2 ppm for both CNTs and CNT–Fe_2O_3. However, increasing the initial phenol concentration in the solution resulted in a decrease in the removal efficiency of the phenol by both CNTs and CNT–Fe_2O_3.

3.3. Adsorption isotherm model

The results obtained on the adsorption of phenol were analyzed by the Langmuir and Freundlich models. The maximum adsorption capacity determined at optimum set of parameters, was used for these adsorption isotherm models. The linear form of Langmuir isotherm is given by Eq. (3), while a plot of C_e/Q_e against C_e. The maximum adsorption capacity (Q_m) and adsorption intensity were determined from the slope and intercept of the straight line [9,13–16,24–41].

It is interesting to note that a good straight line with a high correlation coefficient (99.6%) was obtained for CNF–Fe_2O_3 compared to raw CNFs (98.3%). This shows that impregnation of CNFs has improved the surface homogeneity and Fe_2O_3 nanoparticles were uniformly distributed on the CNF surface.

The adsorption data of phenol were also analyzed by Freundlich model. Based on the Freundlich isotherm model given by the Eq. (4), a plot of $\log Qe$ against $\log C_e$ was generated, which clearly shows the deviation of data from the straight line suggested by the Freundlich model. However, the Freundlich constants, K_F and n; were determined from the best-fit line. The adsorption behavior of adsorbent was best described by the Langmuir adsorption model as compared to the Freundlich model, as shown by their correlation coefficient values in Table 2.

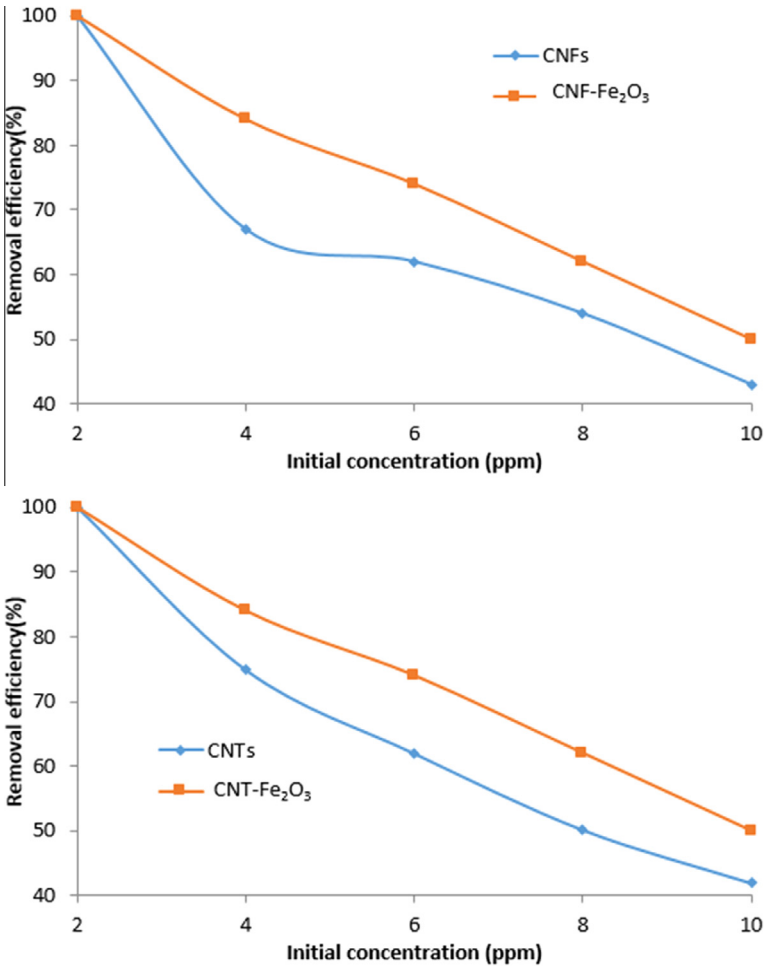

Figure 5 Effect of initial concentration on phenol adsorption using CNFs, CNF–Fe_2O_3 CNTs and CNT–Fe_2O_3.

Table 2 Parameters of Langmuir and Freundlich adsorption isotherm models.

Adsorbent	Langmuir			Freundlich		
	Q_m (mg/g)	K_L (L/mg)	R^2	n	K_F	R^2
CNFs	0.842	2.114	0.983	8.621	0.5888	0.837
CNF–Fe_2O_3	1.684	7.156	0.996	2.747	0.995	0.568
CNTs	1.098	2.4034	0.966	9.615	0.861	0.787
CNT–Fe_2O_3	2.778	6.545	0.994	3.906	1.774	0.660

The adsorption capacities, as determined by the Langmuir isotherm model were 1.684 and 0.842 mg/g for raw CNFs and CNF–Fe_2O_3, respectively. The higher adsorption capacity of CNF–Fe_2O_3 is due to its higher surface areas and more adsorption sites than the raw CNFs. The above analysis also indicates that phenol ions were strongly adsorbed to the surfaces of the CNF–Fe_2O_3 suggesting that impregnation of CNFs Fe_2O_3 have great impact on the adsorption of phenol ions from water.

The results obtained on the adsorption of phenol were analyzed by the Langmuir and Freundlich models. The maximum adsorption capacity determined at optimum set of parameters, was used for these adsorption isotherm models. The linear form of Langmuir isotherm is given by Eq. (3), while a plot of C_e/Q_e against C_e. The maximum adsorption capacity (Q_m) and adsorption intensity were determined from the slope and intercept of the straight line [9,14,17,26]. It is interesting to note that a good straight line with a high correlation coefficient (99.6%) was obtained for CNT–Fe_2O_3 compared to raw CNTs (96.6%). This shows that impregnation of CNTs has improved the surface homogeneity and Fe_2O_3 nanoparticles were uniformly distributed on the CNT surface.

The adsorption data of phenol removal by CNTs were also analyzed by Freundlich model. Based on the Freundlich isotherm model given by the Eq. (4), a plot of $\log Q_e$ against $\log C_e$ was generated, which clearly shows the deviation of data from the straight line suggested by the Freundlich model. However, the Freundlich constants, K_F and n; were determined

from the best-fit line. The adsorption behavior of adsorbent was best described by the Langmuir adsorption model as compared to the Freundlich model, as shown by their correlation coefficient values in Table 2.

The adsorption capacities, as determined by the Langmuir isotherm model were 1.098 and 2.778 mg/g for raw CNTs and CNT–Fe_2O_3, respectively. The higher adsorption capacity of CNT–Fe_2O_3 is due to its higher surface areas and more adsorption sites than the raw CNTs. The above analysis also indicates that phenol ions were strongly adsorbed to the surfaces of the CNT–Fe_2O_3 suggesting that impregnation of CNTs Fe_2O_3 has great impact on the adsorption of phenol ions from water.

4. Conclusion

The potential of raw and ferric oxide impregnated carbon fibers, carbon nanotubes as adsorbents for phenol removal from aqueous solution was successfully demonstrated. The adsorbents were characterized by SEM, TGA, XRD and BET. The surface area was 40.7, 72.4, 155.5 and 227.5 m^2/g for raw CNFs, CNF–Fe_2O_3, CNTs, and CNT–Fe_2O_3, respectively. The phenol removal efficiency of the materials was investigated under optimum solution parameters, such as pH, shaking speed, adsorbent dosage, contact time and initial phenol concentration. The optimum removal from the aqueous solution was achieved at pH 7, 150 rpm shaking speed, 200 mg dosage, 150 min contact time and 2 ppm initial phenol concentration. The data from the phenol adsorption behavior of the carbon based adsorbents were best fitted by the Langmuir adsorption isotherm model, with correlation coefficients of 96.8%, 97.9%, 96.1% and 99.4% for CNF, CNF–Fe_2O_3, CNTs and CNT–Fe_2O_3, respectively. The adsorption capacities, as determined by the Langmuir isotherm model were 0.842, 1.684, 1.098 and 2.778 mg/g for raw CNFs, CNF–Fe_2O_3 CNTs, and CNT–Fe_2O_3, respectively. The higher adsorption capacity by CNT–Fe_2O_3 is mainly attributed to additional adsorption sites due to attachment of iron oxide particles and enhanced interaction to negatively charged oxygen atoms and phenol ions.

Acknowledgment

The authors acknowledge the financial support provided by King Abdulaziz City for Science and Technology (KACST) through the Science and Technology Unit at King Fahd University of Petroleum and Minerals(KFUPM) through project no. AR-30-92.

References

[1] H.H. Fang, O. Chen, Toxicity of phenol towards aerobic biogranules, Water Res. 31 (1997) 2229–2242.
[2] N.N. Dutta, S. Brothakur, R. Baruah, A novel process for recovery of phenol from alkaline wastewater: laboratory study and predesign cost estimate, Water Environ. Res. 70 (1998) 4–9.
[3] K. Juttner, U. Galla, H. Schmieder, Electrochemical approaches to environmental problems in the process industry, Electrochim. Acta 45 (2000) 2575–2954.
[4] M. Tomaszewska, S. Mozia, W. Morawski, Removal of organic matter by coagulation enhanced with adsorption on PAC, Desalination 162 (2004) 79–87.
[5] Z. Lazarova, S. Boyadzhieva, Treatment of phenol-containing aqueous solutions by membrane-based solvent extraction in coupled ultra-filtration modules, Chem. Eng. J. 100 (2004) 129–138.
[6] W. Kujawski, A. Warszawski, W. Ratajczak, W. Capala, Removal of phenol from waste water by different separation techniques, Desalination 163 (2004) 287–296.
[7] N.S. Alderman, A.L.N. Guessan, M.C. Nyman, Effective treatment of PAH contaminated Superfund site soil with the peroxy-acid process, J. Hazardous Mater. 146 (2007) 652–660.
[8] N. Sona, T. Yamamoto, D. Yamamoto, M. Nakaiwa, Degradation of aqueous phenol by simultaneous use of ozone with silica-gel and zeolites, Chem. Eng. Process. 46 (2007) 513–519.
[9] K.A. Halouli, N.M. Drawish, Effect of pH and inorganic salts on the adsorption of phenol from aqueous systems on activated decolorizing charcoal, Sep. Sci. Technol. 30 (1995) 3313–3324.
[10] Y.A. Alhamed, Phenol removal using granular activated carbon from date stones, Bulg. Chem. Comm. 41 (2008) 26–35.
[11] P. Canizares, M. Carmona, O. Baraga, M.A. Rodrigo, Adsorption equilibrium of phenol onto chemical modified activated carbon F400, J. Hazardous Mater. 131 (2006) 243–248.
[12] A. Dabrowski, P. Podkoscielny, Z. Hubicik, M. Barczak, Adsorption of phenolic compounds by activated carbon- a critical review, Chemosphere 58 (2005) 1049–1070.
[13] F.A. Banat, B. Al-Bashir, S. Al-Asheh, O. Hayajneh, Adsorption of phenol by bentonite, Environ. Pollut. 107 (2002) 391–398.
[14] S. Nomanbahay, K. Palanisamy, Removal of heavy metals from industrial waste water using chitosan coated oil palm shell charcoal, Electron. J. Biotechnol. 8 (2005) 43–53.
[15] S. Hydari, H. Sharififard, M. Nabavinia, M. Reza, A comparative investigation on removal performances of commercial activated carbon, chitosan biosorbent and chitosan/activated carbon composite for cadmium, Chem. Eng. J. 193–194 (2012) 276–282.
[16] K. Bhattacharyya, S. Gupta, Pb (II) uptake by kaolinite and montmorillonite in aqueous medium: influence of acid activation of the clays, Colloids Surf. A 277 (2007) 191–200.
[17] A. Ucer, A. Uyanik, S.F. Aygun, Adsorption of Cu(II), Cd(II), Zn(II), Mn(II) and Fe(III) ions by tannic acid immobilised activated carbon, Sep. Purif. Technol. 47 (2006) 113.
[18] Ihsanullah, Fahad Abdulaziz Al-Khaldi, Basil Abusharkh, Mazen Khaled, Muataz Ali Atieh, M.S. Nasser, Taharlaoui, Shilpi Agarwal, Inderjeet Tyagi, Vinod Kumar Gupta, Adsorptive removal of Cadmium (II) ions from liquid phase using acid modified carbon-based adsorbents, J. Mol. Liquids 204 (2015) 248–254.
[19] Hamza A. Ihsanullah, Tawfik A. Asmaly, Tahar Laoui Saleh, Vinod Kumar Gupta, Muataz Ali Atieh, Enhanced adsorption of phenols from liquids by aluminum oxide/carbon nanotubes: Comprehensive study from synthesis to surface properties, J. Mol. Liq. 206 (2015) 176–182.
[20] M. Mansoob Khan, Sajid A. Ansari, M. Ikhlasul Amal, Jintae Lee, Hwan Cho, Highly visible light active Ag@TiO_2 nanocomposites synthesized using an electrochemically active biofilm: a novel biogenic approach, Nanoscale 5 (2013) 4427–4435.
[21] Mohammad Mansoob Khan, Sajid Ali Ansari, MohdOmaish Ansari, B.K. Min, Jintae Lee, Moo Hwan Cho, Biogenic fabrication of Au@CeO_2 nanocomposite with enhanced visible light activity, J. Phys. Chem. C 118 (2014) 9477–9484.
[22] Mohammad Mansoob Khan, Jintae Lee, Moo Hwan Cho, Au@TiO_2nanocomposites for the catalytic degradation of methyl orange and methylene blue: an electron relay effect, J. Ind. Eng. Chem. 20 (2014) 1584–1590.

[23] Sajid Ali Ansari, MohdOmaish Ansari, Jintae Lee, Moo Hwan Cho, Biogenic synthesis, photocatalytic, and photoelectrochemical performance of Ag–ZnO nanocomposite, J. Phys. Chem. C 117 (2013) 27023–27030.
[24] K.D. Samar, Removal of phenolic compounds from aqueous solutions by adsorption onto activated carbons prepared from date stones by chemical activation with FeCl3, J. Eng. 18 (2012) 63–77.
[25] N. Kaushik, T. Mehul, V. Mahesh, J. Pranab, Sorption of phenol from aqueous solution using activated carbon prepared from Manilkarazapota seed, Indian J. Chem. Technol. 15 (2008) 533–540.
[26] Muataz, O. Bakather, B. Tawabini, A. Bukhari, M. Khaled, M. Al-Harthi, M. Fettouhi, F. Abuilaiwi, Removal of chromium (III) from water by using modified and nonmodified carbon nanotubes, J. Nanomater. 232378 (2010) 9.
[27] R. Ramesh, K. Ashok, G.M. Bhalero, S. Ponnusamy, C. Muthamizhchelvan, Synthesis and properties of α-Fe_2O_3nanorods, Cryst. Res. Technol. 45 (9) (2010) 965–968.
[28] V.K. Gupta, R. Jain, A. Mittal, Shilpi Agarwal, Shalini Sikarwar, Photo-catalytic degradation of toxic dye amaranth on TiO_2/UV in aqueous suspensions, Mater. Sci. Eng: C 32 (2012) 12–17.
[29] T.A. Saleh, V.K. Gupta, Column with CNT/magnesium oxide composite for lead (II) removal from water, Environ. Sci. Pollut. Res. 19 (2012) 1224–1228.
[30] V.K. Gupta, S.K. Srivastava, D. Mohan, S. Sharma, Design Parameters for fixed bed reactors of activated carbon developed from fertilizer waste material for the removal of some heavy metal ions, Waste Manage. 17 (1998) 517–522.
[31] V.K. Gupta, Alok Mittal, Jyoti Mittal, Decoloration treatment of a hazardous triarylmethane dye, Light Green SF (Yellowish) by waste material adsorbents, J. Colloid Interface Sci. 342 (2010) 518–527.
[32] V.K. Gupta, Alok Mittal, Dipika Kaur, Arti Malviya, Jyoti Mittal, Adsorption studies on the removal of colouring agent phenol red from wastewater using waste materials as adsorbents, J. Colloid Interface Sci. 337 (2009) 345–354.
[33] Alok Mittal, Arti Malviya, Jyoti Mittal, V.K. Gupta, Adsorptive Removal of hazardous anionic dye 'Congo red' from wastewater using waste materials and recovery by desorption, J. Colloid Interface Sci. 340 (2009) 16–26.
[34] V.K. Gupta, Shilpi Agarwal, Tawfik A. Saleh, Synthesis and characterization of alumina-coated carbon nanotubes and their application for lead removal, J. Hazardous Mat. 185 (2011) 17–23.
[35] V.K. Gupta, Imran Ali, Tawfik A. Saleh, Arunima Nayak, Shilpi Agarwal, Chemical treatment technologies for wastewater recycling – a review, RSC Adv. 2 (2012) 6380–6388.
[36] V.K. Gupta, Alok Mittal, Jyoti Mittal, Removal and recovery of chrysoidine Y from aqueous solutions by waste materials, J. Colloid Interface Sci. 344 (2010) 497–507.
[37] V.K. Gupta, R. Jain, Shilpi Agarwal, M. Shrivastava, Removal of the hazardous dye – Tartrazine by photodegradation on titanium dioxide surface, Mater. Sci. Eng. 31 (2011) 1062–1067.
[38] V.K. Gupta, Arunima Nayak, Cadmium removal and recovery from aqueous solutions by novel adsorbents prepared from orange peel and Fe_2O_3 nanoparticles, Chem. Eng. J. 180 (2012) 81–90.
[39] T.A. Saleh, V.K. Gupta, Photo-catalyzed degradation of hazardous dye methyl orange by use of a composite catalyst consisting of multiwalled carbon nanotubes and titanium dioxide, J. Colloids Interface Sci. 371 (2012) 101–106.
[40] H. Khani, M.K. Rofouei, P. Arab, V.K. Gupta, Z. Vafaei, Multi-walled carbon nanotubes-ionic liquid-carbon paste electrode as a super selectivity sensor: Application to potentiometric monitoring of mercury ion (II), J. Hazard Mater. 183 (2010) 402–409.
[41] V.K. Gupta, M.R. Ganjali, P. Norouzi, H. Khani, A. Nayak, Shilpi Agarwal, Electrochemical analysis of some toxic metals and drugs by ion selective electrodes, Cr. Rev. Anal. Chem. 41 (2011) 282–313.